

# Pressure-tunable structural instabilities in single-layer-trilayer $\text{La}_3\text{Ni}_2\text{O}_7$

Alaska Subedi

*CPHT, CNRS, École polytechnique, Institut Polytechnique de Paris, 91120 Palaiseau, France*

(Dated: December 31, 2024)

Layered nickelates are believed to exhibit superconductivity similar to that found in the cuprates. However, the precise crystal structure of the superconducting phase of the layered nickelates has not been fully clarified. Here, I use first principles calculations to study the pressure dependence of the structural instabilities in the single-layer-trilayer  $\text{La}_3\text{Ni}_2\text{O}_7$ , which is one member of the layered nickelates family that also shows signatures of superconductivity. I find a nearly dispersionless nondegenerate phonon branch in the parent  $P4/mmm$  phase that is unstable along the Brillouin zone edge  $M (\frac{1}{2}, \frac{1}{2}, 0) \rightarrow A (\frac{1}{2}, \frac{1}{2}, \frac{1}{2})$  at all investigated pressures up to 30 GPa. Calculations show additional doubly-degenerate instabilities along the edge  $MA$  at lower pressures. I used group-theoretical analysis to identify the distinct low-symmetry distortions possible due to these instabilities and generated them using the eigenvectors of the unstable modes. Structural relaxations show that the lowest energy structures at 0 and 10 GPa involve condensation of both the nondegenerate and doubly-degenerate instabilities, which is in contrast to the experimental refinements that involve condensation of only the doubly-degenerate branch. I also find that structural distortions are energetically favorable at 20 GPa, contrary to the experiments that do not observe any distortions of the parent  $P4/mmm$  structure at high pressures.

## I. INTRODUCTION

Layered nickelates have been brought into sharp focus since signatures of superconductivity was reported in doped infinite-layer  $\text{NdNiO}_2$  around 15 K in 2019 [1]. This was soon followed by observation of similar superconducting signatures in quintuple-layer  $\text{Nd}_6\text{Ni}_5\text{O}_{12}$  near 13 K [2]. Both findings were made in thin-film samples at ambient pressure. More recently, the exploration of layered nickelates under high pressure has yielded remarkable results. In 2023,  $\text{La}_3\text{Ni}_2\text{O}_7$  was reported to exhibit superconductivity at a notably high temperature of 80 K under pressures exceeding 14 GPa [3]. This high-pressure superconductivity trend has extended to trilayer  $\text{La}_4\text{Ni}_3\text{O}_{10}$  as well [4–8].

Although substantial diamagnetic effects with large volume fraction has been observed in infinite-layer  $\text{Nd}_{0.8}\text{Sr}_{0.2}\text{NiO}_2$  [9] and  $\text{La}_4\text{Ni}_3\text{O}_{10}$  [5, 7], only a weak diamagnetic response suggestive of filamentary or inhomogeneous superconductivity has been detected in  $\text{La}_3\text{Ni}_2\text{O}_7$  [10, 11]. Nevertheless,  $\text{La}_3\text{Ni}_2\text{O}_7$  exhibits linear- $T$  resistivity above onset  $T_c$  [12], motivating similarity with the cuprates high-temperature superconductors. This has prompted extensive experimental and theoretical efforts to elucidate the nature of superconductivity in this material [13–44]. However, the crystal structure of the superconducting phase has not yet been fully determined.

In this regard, it has recently been discovered that  $\text{La}_3\text{Ni}_2\text{O}_7$ , in addition to the bilayer structure, also forms in a single-layer trilayer (SL-TL) phase [45–47]. Although no phase transitions have been observed in thermodynamic experiments in this phase, signatures of superconductivity have been found in resistivity measurements at pressures above 8 GPa [45]. X-ray diffraction experiments find that the ambient-pressure structure of the SL-TL phase can reasonably be refined to structures with  $P4/mmm$ ,  $Fmmm$ ,  $Cmmm$ , or  $Immma$  space groups

[45–47], while the  $P4/mmm$  structure well describes the high-pressure phase above 12.8 GPa [45]. Density functional theory calculations find that the  $Fmmm$  and  $P4/mmm$  structures have the lowest energy for the SL-TL phase at 0 and 16 GPa, respectively [48]. Both experiment and theory find that the electronic states near the Fermi level are derived from nominally Ni  $d_{x^2-y^2}$  narrow and  $d_{x^2-y^2}$  dispersive bands [45, 48–51].

In this paper, I study the structural properties of SL-TL  $\text{La}_3\text{Ni}_2\text{O}_7$  as a function of pressure using first principles calculations. I consider the undistorted model of the SL-TL phase, which has the space group  $P4/mmm$ , and calculate its phonon dispersions. The phonon dispersions at 0 GPa exhibit three unstable branches along the Brillouin edge  $M (\frac{1}{2}, \frac{1}{2}, 0) \rightarrow A (\frac{1}{2}, \frac{1}{2}, \frac{1}{2})$ . The most unstable branch is nondegenerate, whereas the other two are doubly degenerate. As the pressure is increased to 10 GPa, the two lowest of the three unstable branches remain unstable. At 20 GPa, the nondegenerate branch still remains unstable, while the doubly-degenerate branches become stable. I find that the  $P4/mmm$  structure is unstable up to the maximum investigated pressure of 30 GPa, which is contrary to the experimental findings. I used symmetry analysis to enumerate possible distortions due to the two largest instabilities at  $M$  and  $A$ . I generated these structures using the eigenvectors of the unstable phonon modes and relaxed them to obtain their total energies. The lowest energy structures at 0 and 10 GPa involve condensation of both the nondegenerate and doubly-degenerate branches. This is at variance with the experimentally proposed  $Fmmm$  and  $Immma$  structures that involve condensation of only the doubly-degenerate mode. Additionally, the  $Cmmm$  refinement cannot be stabilized in the calculations. At 0 GPa, I find that five distinct lowest-energy structures lie within 0.4 meV/atom. This near degeneracy is increased at 10 GPa, with ten lowest-lying structures having the same

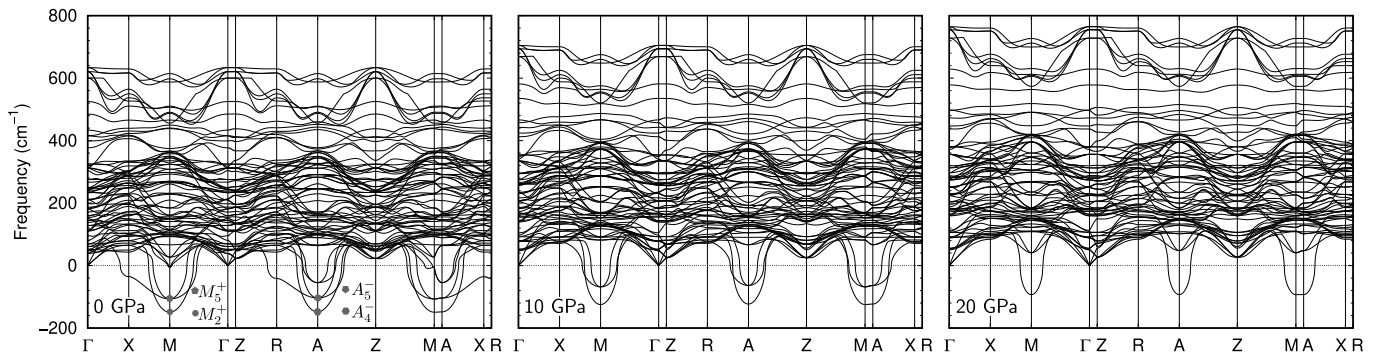


FIG. 1. Calculated phonon dispersions of SL-TL  $\text{La}_3\text{Ni}_2\text{O}_7$  at 0, 10, and 20 GPa in the parent  $P4/mmm$  phase. The high-symmetry points are  $\Gamma$  (0, 0, 0),  $X$  (0,  $\frac{1}{2}$ , 0),  $M$  ( $\frac{1}{2}$ ,  $\frac{1}{2}$ , 0),  $Z$  (0, 0,  $\frac{1}{2}$ ),  $R$  (0,  $\frac{1}{2}$ ,  $\frac{1}{2}$ ), and  $A$  ( $\frac{1}{2}$ ,  $\frac{1}{2}$ ,  $\frac{1}{2}$ ) in terms of the reciprocal lattice vectors. Imaginary frequencies are indicated by negative values.

energy within numerical accuracy. The degeneracy is partially lifted and there are only three nearly degenerate low-energy distortions at 20 GPa. The large degeneracy of the distorted structures is caused by the layered nature of SL-TL  $\text{La}_3\text{Ni}_2\text{O}_7$  and the flatness of the unstable branches, which make the octahedral rotations due to the phonon instabilities uncorrelated especially in the out-of-plane direction. This should manifest as a short coherence length of the distortions in the experiments.

## II. COMPUTATIONAL APPROACH

The phonon dispersions presented in the paper were obtained using density functional perturbation theory as implemented in the QUANTUM ESPRESSO package version 7.3.1 [52]. This is a pseudopotential-based package that uses plane-wave basis set. I used the version 1.0.0 of the ultrasoft pseudopotentials generated by Dal Corso in my calculations [53]. They have the valence configurations La  $5s^25p^66s^{1.5}5d^{1.5}6p^{0.5}$ , Ni  $4s^23d^8$ , and O  $2s^22p^4$ . The calculations were performed within the generalized gradient approximation of Perdew, Burke, and Ernzerhof [54]. The cutoffs of the basis-set and charge-density expansions were set at 60 and 600 Ry, respectively. An  $8 \times 8 \times 2$   $k$ -point grid was used for the Brillouin zone integration with a Marzari-Vanderbilt smearing of 0.01 Ry. The dynamical matrices were calculated on a  $4 \times 4 \times 2$  grid, and the phonon dispersions were obtained using Fourier interpolation. I used the SPGLIB [55], FINDSYM [56], and AMPLIMODES [57] packages in the symmetry analysis of the phonons and distorted structures. The ISOTROPY code [58] was used to determine the order parameter directions due to the unstable phonon modes, and these structures were generated on 192-atom  $2 \times 2 \times 2$  supercells.

The structural relaxation of the distorted structures were performed using the VASP package version 6.4.2 for computational efficiency [59]. These calculations were performed using the projector augmented-wave pseudopotentials with the valence configurations of La

$5s^25p^66s^24f^{0.0001}5d^{0.9999}$ , Ni  $3p^64s^13d^9$ , and O  $2s^22p^4$ . An  $8 \times 8 \times 3$   $k$ -point grid, 500 eV basis-set cutoff, and Methfesse-Paxton smearing of 0.1 eV were used. The spin-orbit interaction was neglected in all calculations.

## III. RESULTS AND DISCUSSION

The ambient pressure x-ray diffraction data of SL-TL  $\text{La}_3\text{Ni}_2\text{O}_7$  has been refined using several different structural models. Puphal *et al.* find that an orthorhombic structure with the space group  $Fmmm$  provides the best refinement, but they also note that structures with the space groups  $Cmmm$ ,  $P4/mmm$ , and  $Imma$  can provide satisfactory refinements [45]. Chen *et al.* report that the  $Cmmm$  structure offers the best fit to their data, which can also be solved using the  $Imma$  structure [46]. Wang *et al.* similarly conclude that the  $Cmmm$  structure provides the best fit to their data [47]. The  $Fmmm$ ,  $Cmmm$ , and  $Imma$  structures of SL-TL  $\text{La}_3\text{Ni}_2\text{O}_7$  all derive from the high-symmetry  $P4/mmm$  structure via atomic displacements along different unstable phonon coordinates. To determine other possible low-symmetry structures, I calculated the phonon dispersions of this material at pressure values of 0, 10, and 20 GPa, which are shown in Fig. 1. The calculated phonon dispersions exhibit instabilities at all investigated pressures along the Brillouin zone edge  $MA$ , which indicates the tetragonal  $P4/mmm$  structure is unstable at these pressures.

At 0 GPa, there are three unstable branches along  $MA$ . The largest instability occurs due to a nondegenerate branch that has the irreducible representations (irreps)  $M_2^+$  and  $A_4^-$  at  $M$  and  $A$ , respectively. The corresponding calculated imaginary frequencies at  $M$  and  $A$  of this branch are  $149i$  and  $148i$   $\text{cm}^{-1}$ . This branch is followed above by a doubly degenerate branch with calculated imaginary frequencies of  $107i$  and  $104i$   $\text{cm}^{-1}$  and irreps of  $M_5^+$  and  $A_5^-$  at  $M$  and  $A$ , respectively. Above this lies another doubly degenerate branch with imaginary frequencies of  $5i$  and  $55i$   $\text{cm}^{-1}$  at  $M$  and  $A$ , respectively. As one can see, the two most unstable branches are al-

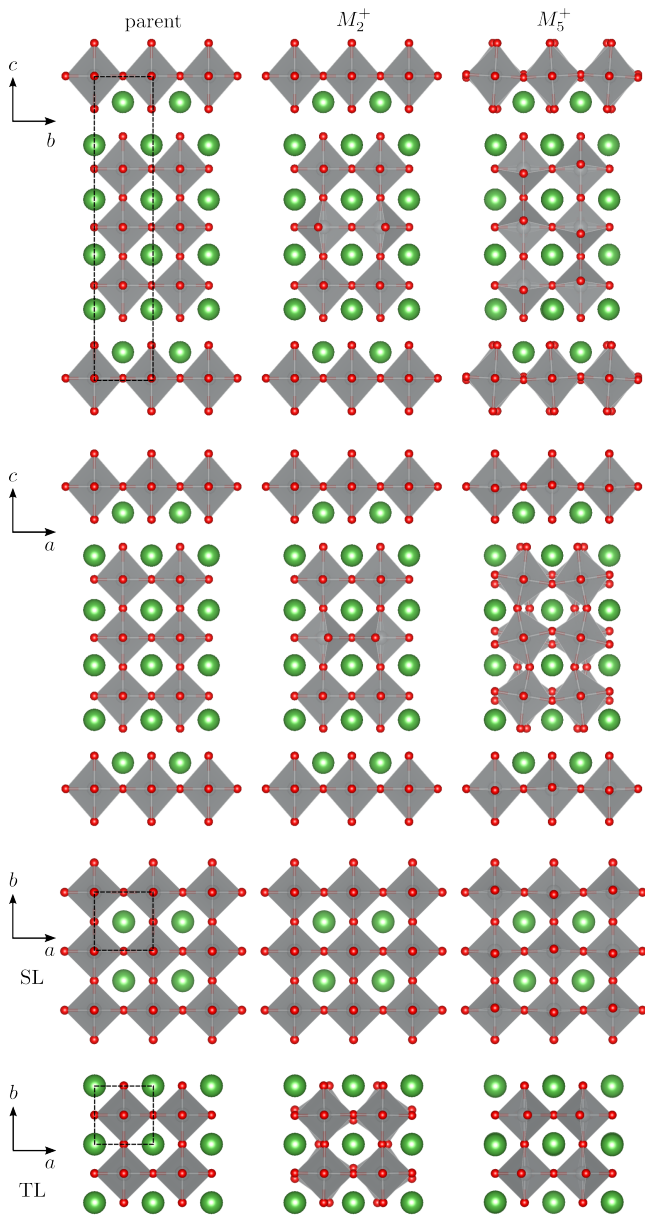


FIG. 2. (Left) The undistorted  $P4/mmm$  structure of SL-TL  $\text{La}_3\text{Ni}_2\text{O}_7$  from different perspectives. (Middle) Structural distortions due to the nondegenerate unstable phonon mode at  $M$  that has the irrep  $M_2^+$ . (Right) Structural distortions due to a component of the doubly-degenerate unstable mode at  $M$  that has the irrep  $M_5^+$ . The corresponding instabilities at  $A$  involve the same atomic displacements but are out of phase in the adjacent unit cells along  $c$ . The unit cell is indicated by the dashed black lines. Green and red spheres indicate La and O, respectively. Ni ions are inside the gray octahedra.

most dispersionless along  $MA$ , but the weakly unstable doubly-degenerate branch shows strong dispersion. Additionally, one offshoot of the more unstable doubly-degenerate branch is unstable throughout the face  $MAXR$ .

As the pressure is increased to 10 GPa, there are only two unstable branches along  $MA$ . The weakly-unstable

doubly degenerate branch of 0 GPa becomes stable at 10 GPa. The calculated imaginary frequencies of the nondegenerate  $M_2^+$  and doubly-degenerate  $M_5^+$  modes decrease to  $125i$  and  $68i$   $\text{cm}^{-1}$ , whereas those of the nondegenerate  $A_4^-$  and doubly-degenerate  $A_5^-$  modes decrease to  $123i$  and  $64i$   $\text{cm}^{-1}$ , respectively. It is noteworthy that the separation between the two unstable branches increases relative to the values calculated at 0 GPa. For example, the difference between the two modes at  $M$  is  $42i$   $\text{cm}^{-1}$  at 0 GPa, but it becomes  $57i$   $\text{cm}^{-1}$  at 10 GPa.

At an even higher pressure of 20 GPa, only the nondegenerate branch is unstable. The calculated imaginary frequencies of the  $M_2^+$  and  $A_4^-$  modes decrease to  $93.0i$  and  $92.9i$   $\text{cm}^{-1}$ , respectively. As the pressure is increased from 0 to 20 GPa, the frequencies of the highest lying phonon branches that are dispersive and correspond to inplane stretching motion of O ions shift up by more than  $130$   $\text{cm}^{-1}$ . The less dispersive branches that lie just below them and correspond to out-of-plane stretching motion of O ions increase their frequencies by between  $60$ – $100$   $\text{cm}^{-1}$ . This smaller increase is not surprising considering the weaker bond in out-of-plane direction due to the presence of interlayer spacing. The frequencies of the rest of the stable branches increase by less than  $50$   $\text{cm}^{-1}$ . Incidentally, I did calculations also at 30 GPa and found that this branch remains unstable, which is surprising considering that Pughal *et al.* report that the structure above  $\sim 12$  GPa has the space group  $P4/mmm$  [45].

The left column of Fig. 2 shows the parent  $P4/mmm$  structure along different directions. The middle column shows the atomic displacements due to the most unstable nondegenerate branch at  $M$  that has the irrep  $M_2^+$  and 0 GPa frequency of  $149i$   $\text{cm}^{-1}$ . This mode mainly involves inplane rotation of the middle layer of the  $\text{NiO}_6$  octahedra within the trilayer. The  $\text{NiO}_6$  octahedra in the outer layers sandwiching the middle layer also show weak inplane rotations out-of-phase along  $c$  that is difficult to discern in the figure. However, the  $\text{NiO}_6$  octahedra within the single layer and La and Ni ions remain fixed. The displacement pattern due to the corresponding mode of this branch at  $A$  is similar, except that they are out of phase by  $180^\circ$  in the neighboring unit cells in the out-of-plane direction.

The right column of Fig. 2 shows the atomic displacements due to one component of the second-most unstable phonon mode at  $M$  at 0 GPa that has the irrep  $M_5^+$  and 0 GPa frequency of  $107i$   $\text{cm}^{-1}$ . This mode involves rotation of all the  $\text{NiO}_6$  octahedra in planes parallel to the  $c$  axis. For the component shown in the figure, the  $\text{NiO}_6$  octahedra within the trilayer rotate in the  $ac$  plane, and these rotations are out-of-phase along the  $b$  axis. Meanwhile, the octahedra within the single layer rotate in the  $bc$  plane, and they propagate out-of-phase along the  $a$  axis. The rotations of the octahedra within the single layer are weaker than those exhibited by the octahedra within the trilayer. Additionally, the outer Ni ions within the trilayer and all the La ions also move by small amounts that are difficult to notice in the figure. The Ni ions and



TABLE I. Isotropy subgroups and corresponding order parameters of  $P4/mmm$  due to the irreps  $M_2^+$ ,  $M_5^+$ ,  $A_4^-$ , and  $A_5^-$ , and their direct sum with each other. Total energies of the structures corresponding to these order parameters directions after structural relaxations at 0 GPa are given in the units of meV/atom relative to the parent  $P4/mmm$  phase. Not all distortions could be stabilized. Structures with " in the energy column relaxed to the preceding order parameter.

Space group	$M_2^+$	$A_4^-$	$M_5^+$	$A_5^-$	Energy
$P4/mmm$					0.0
$P4/mbm$	(a)	(b)			-1.9
$Cmme$			(a, a)	(b, -b)	-3.2
$Fmmm$				(a, a)	-3.2
$Pmna$			(a, 0)	(b, 0)	-3.6
$Imma$				(a, 0)	-3.6
$C2/m$				(a, b)	"
$P4/mbm$	(a)				-3.9
$I4/mcm$		(a)			-3.9
$Cmme$			(a, a)		-4.7
$Ccce$			(a, a)	(b, b)	-4.7
$P2/c$			(a, b)	(c, d)	"
$Cmcm$	(a)			(b, b)	-5.1
$C2/m$		(a)		(b, b)	-5.1
$Pmna$			(a, 0)		-5.2
$Pnna$			(a, 0)	(0, -b)	"
$P2/c$			(a, b)		"
$Pnma$	(a)			(b, 0)	-5.4
$P2_1/m$	(a)			(b, c)	"
$C2/c$		(a)		(b, 0)	-5.4
$P\bar{1}$		(a)		(b, c)	"
$C2/m$	(a)		(b, b)		-6.3
$Cmce$		(a)	(b, b)		-6.3
$P2_1/c$		(a)	(b, c)		-6.5
$Pbcn$		(a)	(b, 0)		-6.7
$P2_1/c$	(a)		(b, 0)		-6.7
$P\bar{1}$	(a)		(b, c)		"

the La ions within the single layer displace along the  $a$  axis, while the La ions within the trilayer displace along the  $b$  axis. These displacements propagate out-of-phase along all three directions.

These unstable phonons of SL-TL  $\text{La}_3\text{Ni}_2\text{O}_7$  generate many possible low symmetry structures. To systematically search for the lowest-energy structure, I used the ISOTROPY package to enumerate the symmetrically distinct structural distortions due to these instabilities. I considered the two lowest-frequency modes at  $M$  and  $A$  that have the irreps  $M_2^+$ ,  $M_5^+$ ,  $A_4^-$ , and  $A_5^-$ , as well as their direct sum with each other. I found 26 distinct order parameters. I generated all these structures using the eigenvectors of the unstable phonon modes and fully relaxed them at specific pressures.

Table I shows the calculated energies of the relaxed structures at 0 GPa. One can first note that the  $Cmmm$  phase refined by Chen *et al.* and Wang *et al.* does not appear in the table [46, 47]. When I took their experimental structures and performed structural relaxation calculations, they relaxed to the  $P4/mmm$  phase.

This suggests that the  $Cmmm$  phase is not energetically favorable. In any case, I find that nineteen distinct distorted structures due to the phonon instabilities could be stabilized that have energies lower than that of the parent  $P4/mmm$  phase. The distorted structures  $A_4^-(a) + M_5^+(b, 0)$  with the space group  $Pbcn$  and  $M_2^+(a) + M_5^+(b, 0)$  with the space group  $P2_1/c$  have the lowest energy, with a value of  $-6.7$  meV/atom relative to the undistorted  $P4/mmm$  phase. These structures involve condensation of the lowest-lying nondegenerate branch at  $A$  and  $M$ , respectively, along with the  $M_5^+(b, 0)$  order parameter direction of the doubly-degenerate unstable mode at  $M$ . The  $Imma$  and  $Fmmm$  structures suggested by the experiments, with the respective order parameters of  $A_5^-(a, 0)$  and  $A_5^-(a, a)$ , derive from condensation of the doubly-degenerate  $A_5^-$  instability. These structures show smaller energy gains of  $-3.6$  and  $-3.2$  meV/atom, respectively. Interestingly, the  $P4/mbm$  phase with the  $M_2^+(a) + A_4^-(b)$  distortion that arises due to condensation of the largest instabilities at  $M$  and  $A$  leads to the smallest energy gain. The largest energy gains involve condensation of the  $M_5^+$  instability in combination with either  $M_2^+$  or  $A_4^-$  instabilities, and there are five of them within 0.4 meV/atom of each other. These structures mainly differ in how the  $\text{NiO}_6$  octahedral rotations due to the phonon instabilities propagate along the three axes.

The five lowest energy structures are not the only group of nearly degenerate structures in Table I. The table shows that condensation of either  $M_2^+$  or  $A_4^-$  along with the doubly-degenerate  $A_5^-$  mode also leads to almost the same energy. This derives from the layered structure of SL-TL  $\text{La}_3\text{Ni}_2\text{O}_7$  and the fact that the unstable branch encompassing both  $M_2^+$  and  $A_4^-$  is almost dispersionless. Since the  $\text{NiO}_6$  octahedra of the SL are not connected to those of the TL along the  $c$  axis, their rotations can be uncorrelated along  $c$ . So the condensation of the dispersionless unstable branch at any out-of-plane periodicity will be nearly degenerate. The close energies of these structures should result in especially short coherence length along the out-of-plane direction, making it difficult to resolve the sample to a single phase in the experiments.

The results of structural relaxations at 10 GPa are shown in Table II. As expected from the instabilities becoming weaker as the pressure is increased, the energy gains due to the distortions at 10 GPa are smaller than those at 0 GPa. Another difference is the larger number—ten—of structures having the lowest energy gain of  $-1.9$  eV/atom. These structures involve condensation of the nondegenerate mode by itself and also in combination with the doubly-degenerate mode. In contrast, at 0 GPa, structures involving condensation of the doubly-degenerate mode at  $A$  and the nondegenerate branch were at least 0.9 meV/atom higher than the structures involving condensation of the doubly-degenerate mode at  $M$  and the nondegenerate branch.

There are further minor differences in the energetics

TABLE II. Total energies of the structures corresponding to the  $M_2^+$ ,  $A_4^-$ ,  $M_5^+$ , and  $A_5^-$  instabilities after structural relaxations at 10 GPa in the units of meV/atom relative to the parent  $P4/mmm$  phase. Not all distortions could be stabilized. Structures with " in the energy column relaxed to the preceding order parameter.

Space group	$M_2^+$	$A_4^-$	$M_5^+$	$A_5^-$	Energy
$P4/mmm$					0.0
$Cmme$			(a, a)	(b, -b)	-0.2
$Pnna$			(a, 0)	(b, 0)	-0.3
$Fmmm$				(a, a)	-0.4
$Imma$				(a, 0)	-0.4
$C2/m$				(a, b)	-0.5
$Pnna$			(a, 0)	(0, -b)	-0.5
$Ccce$			(a, a)	(b, b)	-0.5
$P2/c$			(a, b)	(c, d)	"
$Cmme$			(a, a)		-0.6
$P2/c$			(a, b)		"
$Pmna$			(a, 0)		-0.7
$P4/mbm$	(a)	(b)			-0.9
$P4/mbm$	(a)				-1.9
$I4/mcm$		(a)			-1.9
$Cmcm$	(a)			(b, b)	-1.9
$P2_1/m$	(a)			(b, c)	"
$Pnna$	(a)			(b, 0)	-1.9
$Cmce$		(a)	(b, b)		-1.9
$P2_1/c$		(a)	(b, c)		"
$Pbcn$		(a)	(b, 0)		-1.9
$C2/m$	(a)		(b, b)		-1.9
$P\bar{1}$	(a)		(b, c)		"
$P2_1/c$	(a)		(b, 0)		-1.9
$C2/m$		(a)		(b, b)	-1.9
$P\bar{1}$		(a)		(b, c)	"
$C2/c$		(a)		(b, 0)	-1.9

of the distortions at 0 and 10 GPa even though they involve the same two unstable phonon branches. The  $Pnna$  structure with the order parameter  $M_5^+(a, 0) + A_5^-(0, -b)$  can additionally be stabilized at 10 GPa. Furthermore, the energy gains at 10 GPa due to the condensation of only the doubly-degenerate branch is smaller than those due to the condensation of only the nondegenerate branch. At 0 GPa, two structures due to the condensation of the doubly-degenerate branch are lower in energy than the structures that contain only the distortions due to the nondegenerate branch. The larger separation between the two unstable phonon branches at 10 GPa likely explains the change in the ranking of the relative energies. It is also noteworthy that the additional energy gain due to the condensation of the doubly-degenerate branch on top of the distortions due to the nondegenerate branch is negligible at 10 GPa, which may also be caused by the higher relative position of the doubly-degenerate branch.

At 20 GPa, only the  $M_2^+(a)$ ,  $A_4^-(a)$ , and  $M_2^+(a) + A_4^-(a)$  order parameters with the respective space groups of  $P4/mbm$ ,  $I4/mcm$ , and  $P4/mbm$  are stable after structural relaxations. This is as expected since only the nondegenerate branch is unstable at this pressure. The

TABLE III. Total energies of the structures corresponding to the  $M_2^+$  and  $A_4^-$  instabilities after structural relaxations at 20 GPa in the units of meV/atom relative to the parent  $P4/mmm$  phase. The structures corresponding to the  $M_5^+$  and  $A_5^-$  instabilities relaxed to the parent phase because these modes are stable at this pressure.

Space group	$M_2^+$	$A_4^-$	Energy
$P4/mmm$			0.0
$P4/mbm$	(a)	(b)	-0.2
$P4/mbm$	(a)		-0.4
$I4/mcm$		(a)	-0.4

total energies of these structures are given in Table III. The three distorted structures lie within 0.2 meV/atom of each other, which again reflects the nearly dispersionless nature of the unstable branch along  $MA$ . The  $M_2^+(a)$  and  $A_4^-(a)$  distortions have the lowest energy of  $-0.4$  meV/atom relative to the parent  $P4/mmm$  phase. Despite the small energy gain, the oxygen octahedra in the middle layer of the trilayer rotate by  $16.5^\circ$  in these structures. However, this layer is sandwiched by the outer layers that rotate by less than  $3^\circ$ , and this probably makes it difficult to resolve this structure in the experiments.

#### IV. SUMMARY AND CONCLUSIONS

In summary, I used first principles phonon and structural relaxation calculations to show that the undistorted  $P4/mmm$  model of SL-TL  $\text{La}_3\text{Ni}_2\text{O}_7$  is unstable at all investigated pressures up to 30 GPa. Calculated phonon dispersions show an unstable nondegenerate branch at all pressures along the Brillouin zone edge  $MA$ . At 0 and 10 GPa, there are additionally two and one doubly-degenerate unstable branches, respectively, along this path. I used group-theoretical analysis to find the possible structural distortions that could arise due to the two most unstable phonon modes at  $M$  and  $A$ . Structures corresponding to these order parameter directions were constructed using the eigenvectors of the unstable phonon modes. They were then relaxed at specific pressures to obtain their total energies.

I find that the lowest-energy structures at 0 and 10 GPa involve condensation of both the nondegenerate and doubly-degenerate unstable phonon branches. The  $Fmmm$  and  $Imma$  experimental refinements, which involve the condensation of only the doubly-degenerate mode at  $A$ , lie higher in energy. Another experimentally proposed structure  $Cmmm$  could not be stabilized. The energy gain due to the distortions are relatively small, consistent with the small values of the imaginary frequencies of the unstable phonon modes. At 0 GPa, the lowest-energy structures show an energy gain of  $-6.7$  meV/atom relative to the parent phase. Furthermore there are five distinct structures within 0.4 meV/atom of this value. This degeneracy increases at 10 GPa, where

there are ten distinct structures showing the largest energy gain of  $-1.9$  meV/atom. Only the nondegenerate branch is unstable at 20 GPa. This reduces the degeneracy, with the three distorted structures that are energetically lower than the parent phase lying 0.2 meV/atom of each other. The structural degeneracies occur due to the layered nature of this material and the flatness of the unstable phonon branches, which combine to make the octahedral rotations associated with the phonon instabilities especially uncorrelated in the out-of-plane direction. Furthermore, the nearly dispersionless phonon

instabilities could condense at any intermediate point in the Brillouin zone edge. This should manifest as short coherence length of the out-of-plane structural distortions in the experiments.

## V. ACKNOWLEDGEMENTS

This work was supported by GENCI-TGCC under grant no. A0170913028.

- 
- [1] D. Li, K. Lee, B. Y. Wang, M. Osada, S. Crossley, H. R. Lee, Y. Cui, Y. Hikita, and H. Y. Hwang, Superconductivity in an infinite-layer nickelate, *Nature* **572**, 624 (2019).
- [2] G. A. Pan, D. Ferenc Segedin, H. LaBollita, Q. Song, E. M. Nica, B. H. Goodge, A. T. Pierce, S. Doyle, S. Novakov, D. Córdova Carrizales, A. T. N'Diaye, P. Shafer, H. Paik, J. T. Heron, J. A. Mason, A. Yacoby, L. F. Kourkoutis, O. Erten, C. M. Brooks, A. S. Botana, and J. A. Mundy, Superconductivity in a quintuple-layer square-planar nickelate, *Nature Materials* **21**, 160–164 (2021).
- [3] H. Sun, M. Huo, X. Hu, J. Li, Z. Liu, Y. Han, L. Tang, Z. Mao, P. Yang, B. Wang, J. Cheng, D.-X. Yao, G.-M. Zhang, and M. Wang, Signatures of superconductivity near 80 K in a nickelate under high pressure, *Nature* **621**, 493–498 (2023).
- [4] Q. Li, Y.-J. Zhang, Z.-N. Xiang, Y. Zhang, X. Zhu, and H.-H. Wen, Signature of superconductivity in pressurized  $\text{La}_4\text{Ni}_3\text{O}_{10}$ , *Chinese Physics Letters* **41**, 017401 (2024).
- [5] M. Zhang, C. Pei, X. Du, W. Hu, Y. Cao, Q. Wang, J. Wu, Y. Li, H. Liu, C. Wen, Y. Zhao, C. Li, W. Cao, S. Zhu, Q. Zhang, N. Yu, P. Cheng, L. Zhang, Z. Li, J. Zhao, Y. Chen, H. Guo, C. Wu, F. Yang, S. Yan, L. Yang, and Y. Qi, Superconductivity in trilayer nickelate  $\text{La}_4\text{Ni}_3\text{O}_{10}$  under pressure (2024), arXiv:2311.07423 [cond-mat.supr-con].
- [6] J. Li, C.-Q. Chen, C. Huang, Y. Han, M. Huo, X. Huang, P. Ma, Z. Qiu, J. Chen, X. Hu, L. Chen, T. Xie, B. Shen, H. Sun, D.-X. Yao, and M. Wang, Structural transition, electric transport, and electronic structures in the compressed trilayer nickelate  $\text{La}_4\text{Ni}_3\text{O}_{10}$ , *Sci. China Phys. Mech. Astron* **67**, 117403 (2024).
- [7] Y. Zhu, D. Peng, E. Zhang, B. Pan, X. Chen, L. Chen, H. Ren, F. Liu, Y. Hao, N. Li, Z. Xing, F. Lan, J. Han, J. Wang, D. Jia, H. Wo, Y. Gu, Y. Gu, L. Ji, W. Wang, H. Gou, Y. Shen, T. Ying, X. Chen, W. Yang, H. Cao, C. Zheng, Q. Zeng, J.-g. Guo, and J. Zhao, Superconductivity in pressurized trilayer  $\text{La}_4\text{Ni}_3\text{O}_{10-\delta}$  single crystals, *Nature* **631**, 531–536 (2024).
- [8] H. Nagata, H. Sakurai, Y. Ueki, K. Yamane, R. Matsumoto, K. Terashima, K. Hirose, H. Ohta, M. Kato, and Y. Takano, Pressure-induced superconductivity in  $\text{La}_4\text{Ni}_3\text{O}_{10+\delta}$  ( $\delta = 0.04$  and  $-0.01$ ), *Journal of the Physical Society of Japan* **93**, 095003 (2024).
- [9] S. W. Zeng, X. M. Yin, C. J. Li, L. E. Chow, C. S. Tang, K. Han, Z. Huang, Y. Cao, D. Y. Wan, Z. T. Zhang, Z. S. Lim, C. Z. Diao, P. Yang, A. T. S. Wee, S. J. Pennycook, and A. Ariando, Observation of perfect diamagnetism and interfacial effect on the electronic structures in infinite layer  $\text{Nd}_{0.8}\text{Sr}_{0.2}\text{NiO}_2$  superconductors, *Nature Communications* **13**, 10.1038/s41467-022-28390-w (2022).
- [10] Y. Zhou, J. Guo, S. Cai, H. Sun, P. Wang, J. Zhao, J. Han, X. Chen, Y. Chen, Q. Wu, Y. Ding, T. Xiang, H. K. Mao, and L. Sun, Investigations of key issues on the reproducibility of high- $T_c$  superconductivity emerging from compressed  $\text{La}_3\text{Ni}_2\text{O}_7$  (2024), arXiv:2311.12361 [cond-mat.supr-con].
- [11] J. Wen, Y. Xu, G. Wang, Z.-X. He, Y. Chen, N. Wang, T. Lu, X. Ma, F. Jin, L. Chen, M. Liu, J.-W. Fan, X. Liu, X.-Y. Pan, G.-Q. Liu, J. Cheng, and X. Yu, Probing the Meissner effect in pressurized bilayer nickelate superconductors using diamond quantum sensors (2024), arXiv:2410.10275 [cond-mat.supr-con].
- [12] Y. Zhang, D. Su, Y. Huang, Z. Shan, H. Sun, M. Huo, K. Ye, J. Zhang, Z. Yang, Y. Xu, Y. Su, R. Li, M. Smidman, M. Wang, L. Jiao, and H. Yuan, High-temperature superconductivity with zero resistance and strange-metal behaviour in  $\text{La}_3\text{Ni}_2\text{O}_{7-\delta}$ , *Nature Physics* **20**, 1269–1273 (2024).
- [13] J. Hou, P.-T. Yang, Z.-Y. Liu, J.-Y. Li, P.-F. Shan, L. Ma, G. Wang, N.-N. Wang, H.-Z. Guo, J.-P. Sun, Y. Uwatoko, M. Wang, G.-M. Zhang, B.-S. Wang, and J.-G. Cheng, Emergence of high-temperature superconducting phase in pressurized  $\text{La}_3\text{Ni}_2\text{O}_7$  crystals, *Chinese Physics Letters* **40**, 117302 (2023).
- [14] J. Li, P. Ma, H. Zhang, X. Huang, C. Huang, M. Huo, D. Hu, Z. Dong, C. He, J. Liao, X. Chen, T. Xie, H. Sun, and M. Wang, Pressure-driven right-triangle shape superconductivity in bilayer nickelate  $\text{La}_3\text{Ni}_2\text{O}_7$  (2024), arXiv:2404.11369 [cond-mat.supr-con].
- [15] G. Wang, N. N. Wang, X. L. Shen, J. Hou, L. Ma, L. F. Shi, Z. A. Ren, Y. D. Gu, H. M. Ma, P. T. Yang, Z. Y. Liu, H. Z. Guo, J. P. Sun, G. M. Zhang, S. Calder, J.-Q. Yan, B. S. Wang, Y. Uwatoko, and J.-G. Cheng, Pressure-Induced Superconductivity In Polycrystalline  $\text{La}_3\text{Ni}_2\text{O}_{7-\delta}$ , *Phys. Rev. X* **14**, 011040 (2024).
- [16] X. Ren, R. Sutarto, X. Wu, J. Zhang, H. Huang, T. Xiang, J. Hu, R. Comin, X. J. Zhou, and Z. Zhu, Resolving the Electronic Ground State of  $\text{La}_3\text{Ni}_2\text{O}_{7-\delta}$  Films (2024), arXiv:2409.04121 [cond-mat.supr-con].
- [17] L. Wang, Y. Li, S.-Y. Xie, F. Liu, H. Sun, C. Huang, Y. Gao, T. Nakagawa, B. Fu, B. Dong, Z. Cao, R. Yu,

- S. I. Kawaguchi, H. Kadobayashi, M. Wang, C. Jin, H.-k. Mao, and H. Liu, Structure Responsible for the Superconducting State in  $\text{La}_3\text{Ni}_2\text{O}_7$  at High-Pressure and Low-Temperature Conditions, *Journal of the American Chemical Society* **146**, 7506 (2024), PMID: 38457476.
- [18] M. Zhang, C. Pei, Q. Wang, Y. Zhao, C. Li, W. Cao, S. Zhu, J. Wu, and Y. Qi, Effects of pressure and doping on Ruddlesden-Popper phases  $\text{La}_{n+1}\text{Ni}_n\text{O}_{3n+1}$ , *Journal of Materials Science & Technology* **185**, 147 (2024).
- [19] Z. Liu, H. Sun, M. Huo, X. Ma, Y. Ji, E. Yi, L. Li, H. Liu, J. Yu, Z. Zhang, Z. Chen, F. Liang, H. Dong, H. Guo, D. Zhong, B. Shen, S. Li, and M. Wang, Evidence for charge and spin density waves in single crystals of  $\text{La}_3\text{Ni}_2\text{O}_7$  and  $\text{La}_3\text{Ni}_2\text{O}_6$ , *Sci. China Phys. Mech. Astron.* **66**, 217411 (2023).
- [20] R. Khasanov, T. J. Hicken, D. J. Gawryluk, L. P. Sorel, S. Bötzel, F. Lechermann, I. M. Eremin, H. Luetkens, and Z. Guguchia, Pressure-Induced Split of the Density Wave Transitions in  $\text{La}_3\text{Ni}_2\text{O}_{7-\delta}$  (2024), arXiv:2402.10485 [cond-mat.supr-con].
- [21] X. Chen, J. Choi, Z. Jiang, J. Mei, K. Jiang, J. Li, S. Agrestini, M. Garcia-Fernandez, H. Sun, X. Huang, D. Shen, M. Wang, J. Hu, Y. Lu, K.-J. Zhou, and D. Feng, Electronic and magnetic excitations in  $\text{La}_3\text{Ni}_2\text{O}_7$ , *Nature Communications* **15**, 9597 (2024).
- [22] K. Chen, X. Liu, J. Jiao, M. Zou, C. Jiang, X. Li, Y. Luo, Q. Wu, N. Zhang, Y. Guo, and L. Shu, Evidence of Spin Density Waves in  $\text{La}_3\text{Ni}_2\text{O}_{7-\delta}$ , *Phys. Rev. Lett.* **132**, 256503 (2024).
- [23] Z. Dan, Y. Zhou, M. Huo, Y. Wang, L. Nie, M. Wang, T. Wu, and X. Chen, Spin-density-wave transition in double-layer nickelate  $\text{La}_3\text{Ni}_2\text{O}_7$  (2024), arXiv:2402.03952 [cond-mat.supr-con].
- [24] Z. Luo, X. Hu, M. Wang, W. Wú, and D.-X. Yao, Bilayer Two-Orbital Model of  $\text{La}_3\text{Ni}_2\text{O}_7$  under Pressure, *Phys. Rev. Lett.* **131**, 126001 (2023).
- [25] Y. Zhang, L.-F. Lin, A. Moreo, and E. Dagotto, Electronic structure, dimer physics, orbital-selective behavior, and magnetic tendencies in the bilayer nickelate superconductor  $\text{La}_3\text{Ni}_2\text{O}_7$  under pressure, *Phys. Rev. B* **108**, L180510 (2023).
- [26] Q.-G. Yang, D. Wang, and Q.-H. Wang, Possible  $s_{\pm}$ -wave superconductivity in  $\text{La}_3\text{Ni}_2\text{O}_7$ , *Phys. Rev. B* **108**, L140505 (2023).
- [27] Y. Gu, C. Le, Z. Yang, X. Wu, and J. Hu, Effective model and pairing tendency in bilayer ni-based superconductor  $\text{La}_3\text{Ni}_2\text{O}_7$  (2023), arXiv:2306.07275 [cond-mat.supr-con].
- [28] W. Wú, Z. Luo, D.-X. Yao, and M. Wang, Superexchange and charge transfer in the nickelate superconductor  $\text{La}_3\text{Ni}_2\text{O}_7$  under pressure, *Science China Physics, Mechanics & Astronomy* **67**, 117402 (2024).
- [29] Z. Luo, B. Lv, M. Wang, W. Wú, and D.-X. Yao, High- $T_C$  superconductivity in  $\text{La}_3\text{Ni}_2\text{O}_7$  based on the bilayer two-orbital t-J model, *npj Quantum Materials* **9**, 61 (2024).
- [30] C. Lu, Z. Pan, F. Yang, and C. Wu, Interlayer-Coupling-Driven High-Temperature Superconductivity in  $\text{La}_3\text{Ni}_2\text{O}_7$  under Pressure, *Phys. Rev. Lett.* **132**, 146002 (2024).
- [31] X.-Z. Qu, D.-W. Qu, J. Chen, C. Wu, F. Yang, W. Li, and G. Su, Bilayer  $t-J-J_{\perp}$  Model and Magnetically Mediated Pairing in the Pressurized Nickelate  $\text{La}_3\text{Ni}_2\text{O}_7$ , *Phys. Rev. Lett.* **132**, 036502 (2024).
- [32] Z. Fan, J.-F. Zhang, B. Zhan, D. Lv, X.-Y. Jiang, B. Normand, and T. Xiang, Superconductivity in nickelate and cuprate superconductors with strong bilayer coupling, *Phys. Rev. B* **110**, 024514 (2024).
- [33] Z. Ouyang, J.-M. Wang, J.-X. Wang, R.-Q. He, L. Huang, and Z.-Y. Lu, Hund electronic correlation in  $\text{La}_3\text{Ni}_2\text{O}_7$  under high pressure, *Phys. Rev. B* **109**, 115114 (2024).
- [34] Y.-B. Liu, J.-W. Mei, F. Ye, W.-Q. Chen, and F. Yang,  $s^{\pm}$ -Wave Pairing and the Destructive Role of Apical-Oxygen Deficiencies in  $\text{La}_3\text{Ni}_2\text{O}_7$  under Pressure, *Phys. Rev. Lett.* **131**, 236002 (2023).
- [35] K. Jiang, Z. Wang, and F.-C. Zhang, High-temperature superconductivity in  $\text{La}_3\text{Ni}_2\text{O}_7$ , *Chinese Physics Letters* **41**, 017402 (2024).
- [36] H. Liu, C. Xia, S. Zhou, and H. Chen, Role of crystal-field-splitting and long-range-hoppings on superconducting pairing symmetry of  $\text{La}_3\text{Ni}_2\text{O}_7$  (2023), arXiv:2311.07316 [cond-mat.supr-con].
- [37] Y. feng Yang, G.-M. Zhang, and F.-C. Zhang, Inter-layer valence bonds and two-component theory for high- $t_c$  superconductivity of  $\text{La}_3\text{Ni}_2\text{O}_7$  under pressure (2023), arXiv:2308.01176 [cond-mat.supr-con].
- [38] Y. Zhang, L.-F. Lin, A. Moreo, T. A. Maier, and E. Dagotto, Structural phase transition,  $s_{\pm}$ -wave pairing, and magnetic stripe order in bilayered superconductor  $\text{La}_3\text{Ni}_2\text{O}_7$  under pressure, *Nature Communications* **15**, 2470 (2024).
- [39] V. Christiansson, F. Petocchi, and P. Werner, Correlated Electronic Structure of  $\text{La}_3\text{Ni}_2\text{O}_7$  under Pressure, *Phys. Rev. Lett.* **131**, 206501 (2023).
- [40] H. LaBollita, V. Pardo, M. R. Norman, and A. S. Botana, Electronic structure and magnetic properties of  $\text{La}_3\text{Ni}_2\text{O}_7$  under pressure: active role of the  $\text{Ni-}d_{x^2-y^2}$  orbitals (2024), arXiv:2309.17279 [cond-mat.str-el].
- [41] H. LaBollita, V. Pardo, M. R. Norman, and A. S. Botana, Assessing spin-density wave formation in  $\text{La}_3\text{Ni}_2\text{O}_7$  from electronic structure calculations, *Phys. Rev. Mater.* **8**, L111801 (2024).
- [42] F. Lechermann, J. Gondolf, S. Bötzel, and I. M. Eremin, Electronic correlations and superconducting instability in  $\text{La}_3\text{Ni}_2\text{O}_7$  under high pressure, *Phys. Rev. B* **108**, L201121 (2023).
- [43] F. Lechermann, S. Bötzel, and I. M. Eremin, Electronic instability, layer selectivity, and fermi arcs in  $\text{La}_3\text{Ni}_2\text{O}_7$ , *Phys. Rev. Mater.* **8**, 074802 (2024).
- [44] M. Wang, H.-H. Wen, T. Wu, D.-X. Yao, and T. Xiang, Normal and superconducting properties of  $\text{La}_3\text{Ni}_2\text{O}_7$ , *Chinese Physics Letters* **41**, 077402 (2024).
- [45] P. Puphal, P. Reiss, N. Enderlein, Y.-M. Wu, G. Khalullin, V. Sundaramurthy, T. Priessnitz, M. Knauff, A. Suthar, L. Richter, M. Isobe, P. A. van Aken, H. Takagi, B. Keimer, Y. E. Suyolcu, B. Wehinger, P. Hansmann, and M. Hepting, Unconventional crystal structure of the high-pressure superconductor  $\text{La}_3\text{Ni}_2\text{O}_7$ , *Phys. Rev. Lett.* **133**, 146002 (2024).
- [46] X. Chen, J. Zhang, A. S. Thind, S. Sharma, H. LaBollita, G. Peterson, H. Zheng, D. P. Phelan, A. S. Botana, R. F. Klie, and J. F. Mitchell, Polymorphism in the Ruddlesden-Popper Nickelate  $\text{La}_3\text{Ni}_2\text{O}_7$ : Discovery of a Hidden Phase with Distinctive Layer Stacking, *Journal of the American Chemical Society* **146**, 3640 (2024).
- [47] H. Wang, L. Chen, A. Rutherford, H. Zhou, and W. Xie, Long-range structural order in a hidden phase of ruddlesden-popper bilayer nickelate  $\text{La}_3\text{Ni}_2\text{O}_7$ , *Inorganic Chemistry* **63**, 5020 (2024).



- [48] Y. Zhang, L.-F. Lin, A. Moreo, T. A. Maier, and E. Dagotto, Electronic structure, self-doping, and superconducting instability in the alternating single-layer trilayer stacking nickelates  $\text{La}_3\text{Ni}_2\text{O}_7$ , *Phys. Rev. B* **110**, L060510 (2024).
- [49] S. N. Abadi, K.-J. Xu, E. G. Lomeli, P. Puphal, M. Isobe, Y. Zhong, A. V. Fedorov, S.-K. Mo, M. Hashimoto, D.-H. Lu, B. Moritz, B. Keimer, T. P. Devereaux, M. Heping, and Z.-X. Shen, *Electronic structure of the alternating monolayer-trilayer phase of  $\text{La}_3\text{Ni}_2\text{O}_7$*  (2024), [arXiv:2402.07143](https://arxiv.org/abs/2402.07143) [cond-mat.supr-con].
- [50] H. LaBollita, S. Bag, J. Kapeghian, and A. S. Botana, Electronic correlations, layer distinction, and electron doping in the alternating single-layer-trilayer  $\text{La}_3\text{Ni}_2\text{O}_7$  polymorph, *Phys. Rev. B* **110**, 155145 (2024).
- [51] Z. Ouyang, J.-M. Wang, R.-Q. He, and Z.-Y. Lu, *DFT+DMFT study of correlated electronic structure in the monolayer-trilayer phase of  $\text{La}_3\text{Ni}_2\text{O}_7$*  (2024), [arXiv:2407.08601](https://arxiv.org/abs/2407.08601) [cond-mat.str-el].
- [52] P. Giannozzi, O. Andreussi, T. Brumme, O. Bunau, M. B. Nardelli, M. Calandra, R. Car, C. Cavazzoni, D. Ceresoli, M. Cococcioni, N. Colonna, I. Carnimeo, A. D. Corso, S. de Gironcoli, P. Delugas, R. A. DiStasio, A. Ferretti, A. Floris, G. Fratesi, G. Fugallo, R. Gebauer, U. Gerstmann, F. Giustino, T. Gorni, J. Jia, M. Kawamura, H.-Y. Ko, A. Kokalj, E. Küçükbenli, M. Lazzeri, M. Marsili, N. Marzari, F. Mauri, N. L. Nguyen, H.-V. Nguyen, A. O. de-la Roza, L. Paulatto, S. Poncé, D. Rocca, R. Sabatini, B. Santra, M. Schlipf, A. P. Seitsonen, A. Smogunov, I. Timrov, T. Thonhauser, P. Umari, N. Vast, X. Wu, and S. Baroni, Advanced capabilities for materials modelling with quantum espresso, *Journal of Physics: Condensed Matter* **29**, 465901 (2017).
- [53] A. Dal Corso, Pseudopotentials periodic table: From H to Pu, *Computational Materials Science* **95**, 337 (2014).
- [54] J. P. Perdew, K. Burke, and M. Ernzerhof, Generalized Gradient Approximation Made Simple, *Phys. Rev. Lett.* **77**, 3865 (1996).
- [55] A. Togo and I. Tanaka, SPGLIB: a software library for crystal symmetry search, [arXiv:1808.01590](https://arxiv.org/abs/1808.01590) [cond-mat.mtrl-sci] (2018).
- [56] H. T. Stokes and D. M. Hatch, FINDSYM: program for identifying the space-group symmetry of a crystal, *Journal of Applied Crystallography* **38**, 237 (2005).
- [57] D. Orobengoa, C. Capillas, M. I. Aroyo, and J. M. Perez-Mato, AMPLIMODES: symmetry-mode analysis on the Bilbao crystallographic server, *Journal of Applied Crystallography* **42**, 820 (2009).
- [58] H. T. Stokes, B. J. Campbell, and D. M. Hatch, ISOTROPY software suite, [iso.byu.edu](http://iso.byu.edu).
- [59] G. Kresse and J. Furthmüller, Efficient iterative schemes for ab initio total-energy calculations using a plane-wave basis set, *Phys. Rev. B* **54**, 11169 (1996).